

Cobalt(II), Manganese(IV) Mononuclear and Zinc(II) Symmetric Dinuclear Complexes of an Aliphatic Hydrazone Schiff Base Ligand with Diversity in Coordination Behaviors and Supramolecular Architectures: Syntheses, Structural Elucidations, and Spectroscopic Characterizations

Dipali Sadhukhan,¹ Aurkie Ray,¹ Guillaume Pilet,² Georgina M. Rosair,³ Eugenio Garribba,⁴ Aline Nonat,⁵ Loïc J. Charbonnière,⁵ and Samiran Mitra*¹

¹Department of Chemistry, Jadavpur University, Raja S. C. Mullick Road, Kolkata 700032, West Bengal, India

²Groupe de Cristallographie et Ingénierie Moléculaire Laboratoire des Multimatériaux et Interfaces UMR 5615 CNRS – Université Claude Bernard Lyon 1, Bât. Jules Raulin, 43 bd du 11 Novembre, 1918 69622 Villeurbanne, Cedex, France

³School of Engineering and Physical Sciences, Heriot Watt University, Edinburgh EH14 4AS, UK

⁴Department of Chemistry and Center for Biotechnology Development and Biodiversity Research, University of Sassari, Via Vienna 2, I-07100 Sassari, Italy

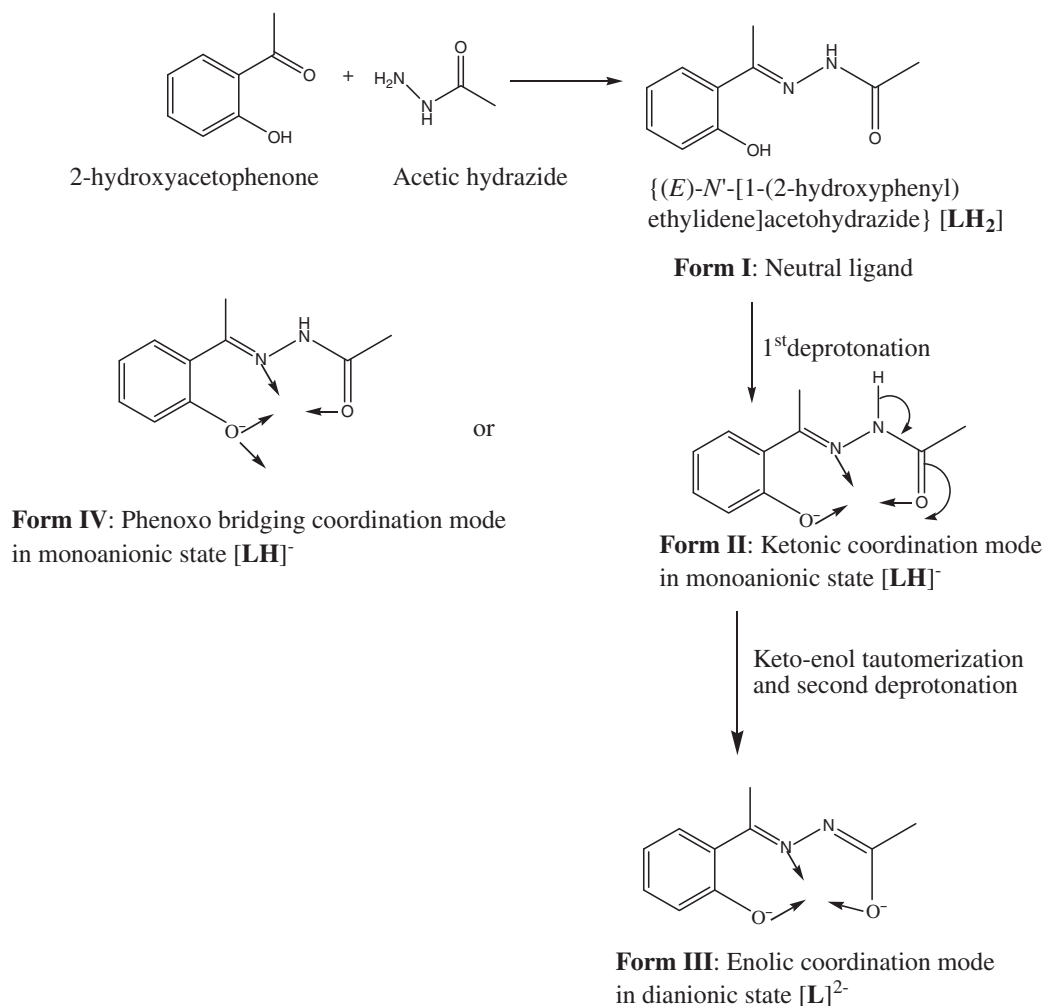
⁵Laboratoire d'Ingénierie Moléculaire Appliquée à l'Analyse, IPHC, UMR 7178, CNRS/UdS, ECPM, 25 rue Becquerel, 67087 Strasbourg Cedex 2, France

Received January 5, 2011; E-mail: smitra_2002@yahoo.com

Three new complexes of cobalt, manganese, and zinc have been synthesized using a hydrazone Schiff base ligand {(*E*)-*N'*-[1-(2-hydroxyphenyl)ethylidene]acetohydrazide} (**LH**₂) produced by the 1:1 condensation of acetic hydrazide and 2-hydroxyacetophenone. The ligand has shown three different coordination modes in the three complexes: a monoanionic tridentate coordination mode with the Co^{II} complex ([Co(**LH**)₂]·CH₃OH, **1**), a dianionic tridentate coordination mode with the Mn^{IV} complex ([Mn(**L**)₂], **2**), and monoanionic μ₂-phenoxo-bridged tridentate coordination mode with the Zn^{II} complex ([Zn(**LH**)(OOCF₃)₂], **3**). All three complexes show interesting supramolecular architectures, especially for **3** a nanoporous supramolecular (4, 4) grid 2D framework is formed. The ligand and the complexes are well characterized by elemental analysis, IR and UV–vis spectroscopy. The spin states of the Co^{II} and Mn^{IV} metal ions and hence the coordination modes of the ligand in these complexes are in good agreement with the EPR spectroscopic data. The fluorescence emission spectra of **LH**₂ and the zinc complex **3** are measured in acetonitrile solution as well as in solid state.

Hydrazones are a special class of Schiff base ligands which contain a secondary amido group (R–CO–NH–) in addition to the azomethine (–C=N–) functionality. It is not easy to make the amido N of hydrazone Schiff bases coordinate to the metal center by deprotonation of the amido N–H proton,¹ but this amido group plays an important role to promote inter- and intramolecular hydrogen-bonding interactions, to stabilize the metal–organic framework and to generate various interesting supramolecular architectures.^{2,3} Moreover the azomethine N, containing a lone pair of electrons in an sp² hybrid orbital, is biologically important.⁴ Additionally, hydrazone metal complexes have also attracted research interest for their possible pharmacological applications,^{5,6} antimicrobial, and antitumor activities.^{7–14} Hydrazone complexes of Ni^{II} were first characterized by Sacconi in 1952.¹⁵ In his report Sacconi stated that the R–CO–NH– group is easier to enolise when R = phenyl, compared with that of the alkyl–CO–NH–. There are plenty of crystal structures of transition-metal complexes of aromatic hydrazones containing an ionic phenolic –OH group in which the Ar–CO–NH– group undergoes

enolisation and second deprotonation, thus behaving as a dianionic ligand as reported by our research group¹⁶ and others.^{17–19} A favorable situation can be created to make the CH₃–CO–NH– group of aliphatic hydrazone Schiff base easily enolisable if all other donor groups of the Schiff base coordinate in their neutral form,^{20,21} or if the metal ion exists in its high oxidation state as shown by Pal et al.²² They have structurally characterized two Ru^{III} complexes with an aliphatic hydrazone ligand *N*-acetyl-*N'*-salicylidenehydrazine (H₂acs). The first one [Ru(acs)(Hacs)] is an octahedral bis chelated complex in which the amido proton of one ligand dissociates, but both the ligand fragments are crystallographically equivalent suggesting a crystallographic static disorder present in the complex. Another complex (PPh₄)[Ru(acs)₂] exhibits the doubly deprotonated ligands coordinating the Ru^{III} center via the enolic form of the amido oxygen. In this report deprotonation of the amido N is assisted by the extensive use of the strong base KOH and stabilization of the coordinated ligands in their dianionic form requires an external cation PPh₄⁺.



Scheme 1. Design of the ligand [LH₂] and its different coordination modes.

In the present work a similar aliphatic hydrazone {(E)-N'-[1-(2-hydroxyphenyl)ethylidene]acetohydrazide} (LH₂) is subjected to complexation with Co^{II}, Mn^{II}, and Zn^{II} precursors, showing three different coordination modes: monoanionic tridentate mode forming a Co^{II} complex, dianionic tridentate mode forming a Mn^{IV} complex and monoanionic μ_2 -phenoxo bridging tridentate mode forming a Zn^{II} complex. The different coordination modes of the ligand LH₂ are automatically stabilized by the oxidation states and geometric requirements of the metal ions (Co^{II}, Mn^{IV}, and Zn^{II}) in the respective complexes, no further assistance by base or any ionic stabilizing agent being required.

Moreover, luminescent metal complexes of salicylaldiminato ligands are being extensively studied after the development of thin layer organic light-emitting diodes (OLED) by Tang and VanSlyke in 1987.²³ Hydrazone ligands containing a salicylaldiminato component provide suitable ligand environment namely a hydroxy group, a coordinating imine N atom and a delocalized π system²⁴ so that their zinc complexes can show excellent luminescence properties in blue, greenish, and red regions.²⁵

In this present work, we have spectroscopically and structurally characterized a new aliphatic hydrazone ligand LH₂ synthesized by 1:1 condensation of acetic hydrazide and

2-hydroxyacetophenone. There are very few structural reports of Cu^{II} and Ru^{III} complexes of quite similar hydrazone ligands synthesized of acetic hydrazide and different substituted/ unsubstituted salicylaldehydes.^{13,26–28} We have prepared three complexes of the ligand with cobalt, manganese, and zinc ions. The X-ray crystal structures of the ligand and the complexes exhibit the unique role of the metal ions to facilitate different ligating behavior of the ligand (Scheme 1). The ligand as well as the complexes exhibits various interesting supramolecular architectures. The mode of ligand coordination to the metal ions is further confirmed by the spin state investigation by EPR spectroscopy of the cobalt and manganese complexes and by the fluorescence spectroscopy of the zinc complex which exhibits blue emission characteristics, typical of μ_2 -phenoxo-bridged zinc–salen complexes.^{29,30}

Experimental

Syntheses. All solvents were of reagent grade and used without further purification. Acetic hydrazide and 2-hydroxyacetophenone were purchased from Aldrich Chemical Co. and used as received. Cobalt perchlorate was prepared by the reaction of cobalt carbonate (E. Merck, India) and 60% perchloric acid (E. Merck, India). To prepare manganous trifluoroacetate, aqueous solution of manganous sulfate was

treated with aqueous sodium carbonate solution in 1:2 molar ratio, the light pink precipitate of manganous carbonate was collected by filtration and 60% trifluoroacetic acid (E. Merck, India) was added immediately within the precipitate. Zinc trifluoroacetate was prepared by treatment of zinc carbonate (E. Merck, India) with 60% trifluoroacetic acid (E. Merck, India). In all the cases the metal perchlorate and trifluoroacetate solutions were filtered through a fine glass-frit and evaporated on a steam bath and preserved in a CaCl₂ desiccator for further use.

Synthesis of the Hydrazone Ligand {(E)-N'-[1-(2-hydroxyphenyl)ethylidene]acetohydrazide} [LH₂]. The ligand LH₂ {(E)-N'-[1-(2-hydroxyphenyl)ethylidene]acetohydrazide} was prepared by the condensation of acetic hydrazide (0.74 g, 10 mmol) with 2-hydroxyacetophenone (1.362 g, 10 mmol) in the presence of a catalytic amount of glacial acetic acid in methanol medium (200 mL). On refluxing the methanolic solution for 5 h a colorless solution was observed. The solvent was removed under reduced pressure and the white residue was purified by recrystallization from methanol from which colorless shiny crystals were obtained. Yield 0.177 g (92%). Elemental analysis. Found: C, 62.58; H, 6.23; N, 14.49%. Calcd for C₁₀H₁₂N₂O₂ (192.1): C, 62.49; H, 6.29; N, 14.57%. Main FT-IR bands. $\nu_{C=N}$ 1667, $\nu_{C=O}$ 1608, ν_{N-H} 3100 cm⁻¹. Main UV-vis bands. $\pi-\pi^*$ 246, $n-\pi^*$ 320 nm.

Synthesis of [Co(LH₂)₂·CH₃OH (1). Co(ClO₄)₂·xH₂O (0.381 g, 1.5 mmol) was dissolved in 20 mL methanol. 20 mL warm methanolic solution of the Schiff base LH₂ (0.178 g, 1 mmol) was added to the former. The mixture was allowed to stir for 0.5 h with heating at 60 °C. The dark brown solution was kept at room temperature. Orange plate shaped single crystals suitable for X-ray diffraction were obtained within two days. Crystals were isolated by filtration and were air-dried. Yield: 0.201 g (85%). Elemental analysis. Found: C, 53.17; H, 5.38; N, 11.75%. Calcd for C₂₁H₂₆CoN₄O₅ (473.39): C, 53.23; H, 5.49; N, 11.83%. Main FT-IR bands. $\nu_{C=N}$ 1591, $\nu_{C=O}$ 1544, ν_{N-H} 2928, ν_{Co-N} 459 cm⁻¹. Main UV-vis bands. $\pi-\pi^*$ 300, $n-\pi^*$ 382, LMCT 238 nm.

Synthesis of [Mn(LH₂)₂ (2). Mn(OOCCF₃)₂·xH₂O (0.4215 g, 1.5 mmol) was dissolved in 20 mL acetonitrile. 20 mL warm methanolic solution of the Schiff base LH₂ (0.178 g, 1 mmol) was added to the former. The mixture was allowed to stir for 1 h with heating at 60 °C. The resulting dark brown solution was kept undisturbed at room temperature for slow evaporation of solvent. Red plate shaped single crystals suitable for X-ray diffraction were obtained after one week. Crystals were isolated by filtration and were air-dried. Yield: 0.178 g (82%). Elemental analysis. Found: C, 55.05; H, 4.46; N, 12.75%. Calcd for C₂₀H₂₀MnN₄O₄ (435.34): C, 55.13; H, 4.59; N, 12.86%. Main FT-IR bands. $\nu_{C=N}$ 1577, $\nu_{C=O}$ 1542, ν_{Mn-N} 444 cm⁻¹. Main UV-vis bands. $\pi-\pi^*$ 291, $n-\pi^*$ 350, LMCT 221, ⁴A_{2g} → ⁴T_{2g} 553, ⁴A_{2g} → ⁴T_{1g}(F) 419 nm.

Synthesis of [Zn(LH)(OOCCF₃)₂ (3). Zn(OOCCF₃)₂·xH₂O (0.4371 g, 1.5 mmol) was dissolved in 20 mL acetonitrile. 20 mL warm methanolic solution of the Schiff base LH₂ (0.178 g, 1 mmol) was added to the former. The mixture was allowed to stir for 1 h with heating at 60 °C. The colorless solution was kept undisturbed at room temperature for slow evaporation of solvent. Colorless cubic single crystals suitable for X-ray diffraction were obtained after one week. Crystals

were isolated by filtration and were air-dried. Yield: 0.5839 g (79%). Elemental analysis. Found: C, 38.79; H, 2.80; N, 7.38%. Calcd for C₂₄H₂₂F₆N₄O₈Zn₂ (739.21): C, 38.96; H, 2.98; N, 7.57%. Main FT-IR bands. $\nu_{C=N}$ 1624, $\nu_{C=O}$ 1600, ν_{N-H} 3058, ν_{Zn-N} 438, ν_{C-F} 1189, ν_{COO^-} (asym) 1685 cm⁻¹. Main UV-vis bands. $\pi-\pi^*$ 252; $n-\pi^*$ 357 nm.

Physical Measurements. The Fourier transform infrared spectra were recorded in the range 4000–400 cm⁻¹ on a Perkin-Elmer RX I FT-IR spectrophotometer with solid KBr pellets. The electronic spectra in HPLC grade acetonitrile were recorded at 300 K on a Perkin-Elmer Lambda 40 (UV-vis) spectrometer in a 1 cm quartz cuvette in the range 800–200 nm. C, H, and N microanalyses were carried out with a Perkin-Elmer 2400 II elemental analyzer. ¹H NMR spectrum of LH₂ was recorded on a BRUKER 300 MHz FT-NMR spectrometer using trimethylsilane as an internal standard in CDCl₃. EPR spectra were recorded at room temperature or at 100 K with an X-band (9.15 GHz) Varian E-9 spectrometer. The steady state fluorescence emission spectra for LH₂ and **3** were recorded in acetonitrile medium at 25 °C on a Perkin-Elmer LS55 luminescence spectrometer. The fluorescence quantum yields (ϕ) were calculated with reference to quinine sulfate in 0.5 M sulfuric acid with a known ϕ_r of 0.546 when excited at 356 nm at 25 °C using the following equation:

$$\phi_x/\phi_r = [I_x/I_r] \times [A_r/A_x] \times [\lambda_r/\lambda_x] \times [\eta_x/\eta_r]^2 \quad (1)$$

Here, subscripts *x* and *r* refer to the unknown and reference solutions, ϕ is a quantum yield, *A* is a calculated optical density, λ is excitation wavelength, *I* is the area under the emission curve which was integrated using the software available in the instrument and η is the index of refraction of the solvent.³¹ The fluorescence lifetime of **3** was determined by time-correlated single-photon counting using a nano-LED excitation source at 370 nm and TBX-04 detector (both IBH, U.K.). The decays were analyzed using IBH DAS-6 decay analysis software.

Steady state emission and excitation spectra in the solid state were recorded on a Horiba Jobin Yvon Fluorolog 3 spectrometer working with a 450W Xe lamp and fitted with an integrating sphere Quanta- Φ from Horiba. Detection was performed with a Hamamatsu R928 photomultiplier. All spectra were corrected for the instrumental functions. When necessary, a 350 nm cut-off filter was used to eliminate the second generation harmonic artifacts.

Luminescence quantum yields were determined using an absolute method with an integrating sphere Quanta- Φ from Horiba. The quantum yield in the absolute method can be calculated by eq 2

$$\phi = \frac{N_{\text{emission}}}{N_{\text{absorption}}} = \frac{\int \frac{\lambda}{hc} \{I_{\text{em}}^{\text{sam}}(\lambda) - I_{\text{em}}^{\text{ref}}(\lambda)\} d\lambda}{\int \frac{\lambda}{hc} \{I_{\text{ex}}^{\text{ref}}(\lambda) - I_{\text{ex}}^{\text{sam}}(\lambda)\} d\lambda} \quad (2)$$

where *N*_{absorption} is the number of photons absorbed by a sample and *N*_{emission} is the number of photons emitted from a sample, λ is the wavelength, *h* is Planck's constant, *c* is the velocity of light, *I*_{ex}^{sam} and *I*_{ex}^{ref} are the integrated intensities of the excitation light with and without a sample, respectively, *I*_{em}^{sam} and *I*_{em}^{ref} are the photoluminescence intensities with and without a sample,

respectively.³² This method has been described in detail by Rohwer and Martin.³³

X-ray Crystallography. The X-ray diffraction data of **LH₂** were collected on a colorless cubic single crystal (0.08 mm × 0.24 mm × 0.25 mm) using a Nonius Kappa CCD diffractometer³⁴ containing area detector and graphite monochromator with Mo K α radiation ($\lambda = 0.71073$ Å). Empirical absorption corrections were carried out by multi scan technique. Data reduction was performed with DENZO/SCALEPACK program³⁵ The structures were solved by direct method using the program SIR97³⁶ and refined with the program CRYSTALS.³⁷ All non-hydrogen atoms were refined anisotropically by full-matrix least-squares based on *F*. All other H atoms were generated geometrically and were included in the refinement in the riding model approximation. The lattice constants were refined by least-square refinement using 7373 total reflections ($2.630^\circ < \theta < 27.372^\circ$), 2037 unique reflections ($R_{\text{int}} = 0.031$). Structure solution and refinement based on 1327 reflections with $I > 3\sigma(I)$ and 128 parameters gave final $R = 0.0395$, $wR = 0.0415$, and $S = 1.0955$. The X-ray diffraction experiment of **1** was carried out at 293 K on an orange plate shaped single crystal (0.02 mm × 0.05 mm × 0.10 mm). The intensity data of **1** were collected with an Oxford Diffraction XCALIBUR diffractometer³⁴ containing area detector and graphite monochromator using ω scan technique with Mo K α radiation ($\lambda = 0.71073$ Å) and data reduction was performed with CrysAlis RED program.³⁸ The structures were solved by direct method using the program SIR97³⁹ and refined with the program CRYSTALS.³⁷ All non-hydrogen atoms were refined anisotropically by full-matrix least-squares based on *F*. The lattice constants were refined by least-square refinement using 8389 total reflections ($3^\circ < \theta < 30^\circ$) and 4766 independent reflections ($R_{\text{int}} = 0.058$). Structure solution and refinement based on 2723 reflections with $I > 2\sigma(I)$ and 280 parameters gave final $R = 0.0627$, $wR = 0.0514$, and $S = 1.11$. X-ray diffraction of **2** was carried out at 100(2) K on a red plate shaped single crystal (0.42 mm × 0.24 mm × 0.06 mm). The selected crystal was mounted on a X8 ApexII Bruker area diffractometer with Mo K α radiation ($\lambda = 0.71073$ Å). Data reduction was performed with SAINT program.³⁹ The lattice constants were refined by least-square refinement using 15256 total reflections ($1.54^\circ < \theta < 25.97^\circ$), 3558 unique reflections ($R_{\text{int}} = 0.0532$). Structure solution and refinement based on 3558 reflections with $I > 2\sigma(I)$ and 266 parameters gave final $R = 0.0389$, $wR = 0.0787$, and $S = 1.021$. Data collection and data reduction were done with the APEX 2⁴⁰ and SAINT³⁹ programs respectively. The structures were solved by direct methods using the SHELXS-97 and refined by full-matrix least-squares methods in SHELXL-97.⁴¹ All non-hydrogen atoms were refined anisotropically by full-matrix least-squares based on *F*². The H atoms were generated geometrically and were included in the refinement in the riding model approximation. The X-ray diffraction experiment of **3** was carried out at 293 K on a colorless cubic single crystal (0.11 mm × 0.11 mm × 0.12 mm). The intensity data of **3** were collected with an Oxford Diffraction XCALIBUR diffractometer³⁴ containing area detector and graphite monochromator using multi scans with Mo K α radiation ($\lambda = 0.71073$ Å). Empirical absorption corrections were carried out by multi scans using

DENZO/SCALEPACK.³⁵ Data reduction was performed with CrysAlis RED.³⁸ The structures were solved by direct method using the program SIR97³⁶ and refined with the program CRYSTALS.³⁷ All non-hydrogen atoms were refined anisotropically by full-matrix least-squares based on *F*. All other H atoms were generated geometrically and were included in the refinement in the riding model approximation. The lattice constants were refined by least-square refinement using 16338 total reflections ($3.459^\circ < \theta < 29.290^\circ$), 3501 unique reflections ($R_{\text{int}} = 0.037$). Structure solution and refinement based on 2119 reflections with $I > 3\sigma(I)$ and 199 parameters gave final $R = 0.0325$, $wR = 0.0355$, and $S = 1.07$. Selected crystallographic data, experimental conditions, and relevant features of the structural refinements for all the complexes are summarized in Table 1.

Crystallographic data have been deposited with Cambridge Crystallographic Data Centre: Deposition number CCDC-805161, 790364, 790366, and 790365 for **LH₂**, **1**, **2**, and **3**. Copies of the data can be obtained free of charge via <http://www.ccdc.cam.ac.uk/conts/retrieving.html> (or from the Cambridge Crystallographic Data Centre, 12, Union Road, Cambridge, CB2 1EZ, U.K.; Fax: +44 1223 336033; e-mail: deposit@ccdc.cam.ac.uk).

Results and Discussion

Fourier Transform Infrared Spectra. The IR spectra of the complexes **1–3** were analyzed in comparison with that of the free ligand **LH₂** in the region 4000–400 cm⁻¹. The main FT-IR bands are listed in Table 2 and a representative IR spectrum of **2** is depicted in Figure S1. In the IR spectrum of the free hydrazone ligand, imine ($\nu_{\text{C=N}}$) stretching band appeared at 1667 cm⁻¹, but for the complexes the characteristic imine bands were observed at lower stretching frequencies: 1591, 1577, and 1624 cm⁻¹ respectively for the complexes **1–3**, indicating the coordination of the imine nitrogen atom to the metal center.^{42,43} $\nu_{\text{C=O}}$ signal for the amide moiety (–CONH–) centered at 1608 cm⁻¹ in **LH₂** undergoes lower frequency shift to 1544, 1542, and 1600 cm⁻¹ in complexes **1–3** respectively. The broad band around 3100 cm⁻¹ for N–H stretching in the spectrum of the ligand is shifted to 2928 and 3058 cm⁻¹ in **1** and **3** confirming the possibility of the amide moiety to coordinate to the metal center in its ketonic form and the amide protons to be involved in hydrogen-bonding interactions, but the $\nu_{\text{N-H}}$ signal is absent in **2**, suggesting the possibility of second deprotonation of the ligand. Ligand coordination to the metal center can further be substantiated by prominent $\nu_{\text{M-N}}$ bands (M = Co, Mn, and Zn for **1**, **2**, and **3** respectively) at 459, 444, and 438 cm⁻¹ in the respective spectra of the complexes **1–3**.⁴⁴ In the spectrum of **3** some new bands appeared which were not present in the spectra of the free ligand as well as in **1** and **2** and can be attributed to various stretching frequencies of trifluoroacetate anion. Strong C–F stretching bands at 1189 cm⁻¹ and asymmetric COO⁻ stretching at 1685 cm⁻¹ indicate the presence of trifluoroacetate moiety in **3**,⁴⁵ also confirmed by the crystal structure.

Electronic Spectra. The electronic spectra for complexes **1–3** were analyzed in comparison with that of the free ligand **LH₂** in the region 800–200 nm in HPLC grade acetonitrile as well as in solid state using paraffin oil matrix. The observed

Table 1. Crystal Structure Parameters of **LH₂**, **1**, **2**, and **3**

	Compounds			
	LH₂	1	2	3
Formula	C ₁₀ H ₁₂ N ₂ O ₂	C ₂₁ H ₂₆ CoN ₄ O ₅	C ₂₀ H ₂₀ MnN ₄ O ₄	C ₂₄ H ₂₂ F ₆ N ₄ O ₈ Zn ₂
Mol. weight/g mol ⁻¹	192.22	473.39	435.34	739.21
T/K	293	293	100(2)	293
Wavelength/Å	0.71073	0.71073	0.71073	0.71073
Crystal system	Monoclinic	Triclinic	Triclinic	Monoclinic
Space group	P 1 21/c 1	<i>P</i> $\bar{1}$ (No. 2)	<i>P</i> $\bar{1}$	C2/c (No. 15)
<i>a</i> /Å	7.5632(12)	8.182(1)	7.3651(17)	21.311(5)
<i>b</i> /Å	13.637(2)	10.559(1)	10.094(3)	9.012(5)
<i>c</i> /Å	9.6739(15)	12.456(2)	13.558(3)	15.578(5)
α /°	90	73.12(1)	80.635(8)	90
β /°	103.412(2)	88.90(1)	79.573(8)	109.306(5)
γ /°	90	88.67(1)	72.508(8)	90
<i>V</i> /Å ³	970.6(3)	1029.4(2)	939.1(4)	2824(2)
<i>Z</i>	4	2	2	4
<i>D</i> /g cm ⁻³	1.32	1.527	1.539	1.739
μ /mm ⁻¹	0.93	0.876	0.739	1.793
<i>F</i> (000)	408	494	450	1488
Crystal size/mm ³	0.08 × 0.24 × 0.25	0.02 × 0.05 × 0.10	0.42 × 0.24 × 0.06	0.11 × 0.11 × 0.12
θ range	2.630 to 27.372°	3 to 30°	1.54 to 25.97°	3.459 to 29.290°
Reflections collected	7373	8389	15256	16338
Ind. reflections	2037	4766	3558	3501
<i>R</i> (int)	0.031	0.058	0.0532	0.037
Reflections used	1327	2723	3558	2119
Parameters refined	128	280	266	199
<i>S</i>	1.0955	1.11	1.021	1.07
Final <i>R</i> indices	<i>R</i> = 0.0395, <i>wR</i> = 0.0415 [<i>I</i> > 3 σ (<i>I</i>)]	<i>R</i> = 0.0627, <i>wR</i> = 0.0514 [<i>I</i> > 2 σ (<i>I</i>)]	<i>R</i> = 0.0389, <i>wR</i> = 0.0787 [<i>I</i> > 2 σ (<i>I</i>)]	<i>R</i> = 0.0325, <i>wR</i> = 0.0355 [<i>I</i> > 3 σ (<i>I</i>)]
$\Delta\rho_{\max}$ and $\Delta\rho_{\min}$ /e Å ⁻³	0.23 and -0.14	0.96 and -0.70	0.341 and -0.383	0.67 and -0.47

Table 2. Important Band Positions of FT-IR and UV-vis Spectra

	Compounds			
	LH₂	1	2	3
FT-IR/cm ⁻¹	$\nu_{\text{C=N}}$ 1667 $\nu_{\text{C=O}}$ 1608 $\nu_{\text{N-H}}$ 3100	$\nu_{\text{C=N}}$ 1591 $\nu_{\text{C=O}}$ 1544 $\nu_{\text{N-H}}$ 2928 $\nu_{\text{Co-N}}$ 459	$\nu_{\text{C=N}}$ 1577 $\nu_{\text{C=O}}$ 1542 $\nu_{\text{Mn-N}}$ 444	$\nu_{\text{C=N}}$ 1624 $\nu_{\text{C=O}}$ 1600 $\nu_{\text{N-H}}$ 3058 $\nu_{\text{Zn-N}}$ 438 $\nu_{\text{C-F}}$ 1189 ν_{COO^-} (asym) 1685
UV-vis in CH ₃ CN/nm	π - π^* 246 n- π^* 320	π - π^* 300 n- π^* 382 LMCT 238	π - π^* 291 n- π^* 350 LMCT 221 $^4\text{A}_{2g} \rightarrow ^4\text{T}_{2g}$ 553 $^4\text{A}_{2g} \rightarrow ^4\text{T}_{1g}(\text{F})$ 419	π - π^* 252 n- π^* 357
UV-vis in nujol/nm	π - π^* 250 n- π^* 324	π - π^* 304 n- π^* 388 LMCT 242	π - π^* 296 n- π^* 356 LMCT 228 $^4\text{A}_{2g} \rightarrow ^4\text{T}_{2g}$ 558 $^4\text{A}_{2g} \rightarrow ^4\text{T}_{1g}(\text{F})$ 426	π - π^* 265 n- π^* 364

UV-vis bands in both phases are listed in Table 2 and the spectra in CH₃CN are shown in Figure 1. In CH₃CN solution the UV-vis spectrum of the Schiff base ligand **LH₂** exhibited two intense absorption bands at 246 and 320 nm which can be attributed to $\pi \rightarrow \pi^*$ (C=N) and n $\rightarrow \pi^*$ transitions possibly

relating to phenoxide lone pair and the π^* orbital of imine i.e., [lp(phenoxide) $\rightarrow \pi^*$ (imine)] within the Schiff base ligand. The ligand-centered transition bands of **LH₂** at 246 and 320 nm may have suffered large bathochromic shifts in the spectra of the complexes appearing at 300 and 382 nm in **1**, at 291 and

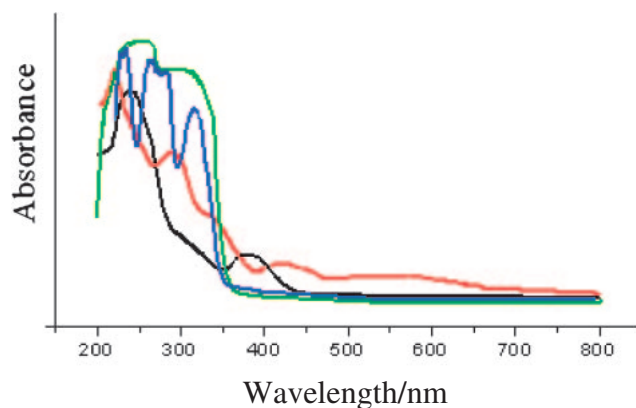


Figure 1. UV-vis spectra of LH_2 (green), **1** (blue), **2** (red), and **3** (black).

350 nm (shoulder) in **2**, and at 252 and 357 nm in **3**. The sharp and intense bands at 238 nm in **1** and 221 nm in **2** can be considered as a $L \rightarrow M$ charge-transfer transition since no band in this region was observed in the spectra of the free ligand LH_2 and the zinc complex **3**. The LMCT band for Co^{II} complexes are generally expected in the visible region^{46,47} but for **1** it is significantly blue shifted due to the presence of strong axial donor group (imine) which destabilizes the metal d_{z^2} orbital, thus creating a larger energy gap between π^* (imine) and d_{z^2} (metal).⁴⁸ For **2** the LMCT band position is in good agreement with a previously reported Mn^{IV} system.⁴⁹ The $d \rightarrow d$ transition is only clearly visible and well resolved. For the octahedral Mn^{IV} system three possible spin allowed $d \rightarrow d$ transitions are: ${}^4A_{2g} \rightarrow {}^4T_{2g}$, ${}^4A_{2g} \rightarrow {}^4T_{1g}(\text{F})$, and ${}^4A_{2g} \rightarrow {}^4T_{1g}(\text{P})$.⁵⁰ Two broad bands of relatively weaker intensity centered at 553 and 419 nm in **2** can be assigned to ${}^4A_{2g} \rightarrow {}^4T_{2g}$ and ${}^4A_{2g} \rightarrow {}^4T_{1g}(\text{F})$.⁵¹ The ${}^4A_{2g} \rightarrow {}^4T_{1g}(\text{P})$ transition may have been obscured by the $[\text{lp}(\text{phenoxide}) \rightarrow \pi^*(\text{imine})]$ charge-transfer band. The unambiguous assignment of $d \rightarrow d$ transitions in **1** is very difficult due to very weak absorption intensity of the $d-d$ bands in the visible region in an octahedral Co^{II} complex.

The UV-vis bands obtained in solid state for all the compounds are in good agreement with the solution phase spectra (Table 2). The small shifts in solution phase are due to solvatochromic effect of the polar solvent (CH_3CN) used.

Cyclic Voltammetric Studies of 1 and 2. Redox properties of **1** and **2** were investigated by cyclic voltammetry in HPLC grade acetonitrile medium with tetrabutylammonium perchlorate as supporting electrolyte at a scan rate of 0.05 V s^{-1} . The cyclic voltammogram of **1** and **2** are depicted in Figures 2a and 2b respectively. The Co^{II} complex **1** showed an irreversible reductive response at -0.71 V . The Mn^{IV} complex **2** showed a single electron $\text{Mn}^{\text{IV}} \rightarrow \text{Mn}^{\text{III}}$ reduction at -0.064 V and during the anodic scan the reverse oxidative response was found at $+0.086 \text{ V}$. Another oxidation peak was present in the voltammogram of **2** at more positive potential ($+1.252 \text{ V}$) which probably corresponds to $\text{L}^{2-} \rightarrow \text{L}^-$ oxidation and was absent in the voltammogram of **1**. This oxidation peak at higher positive potential indicates that the ligand exists in a lower oxidation state in **2** than in **1**. Additionally the more negative reduction potential of **1** compared to **2** indicates that the Co ion is much

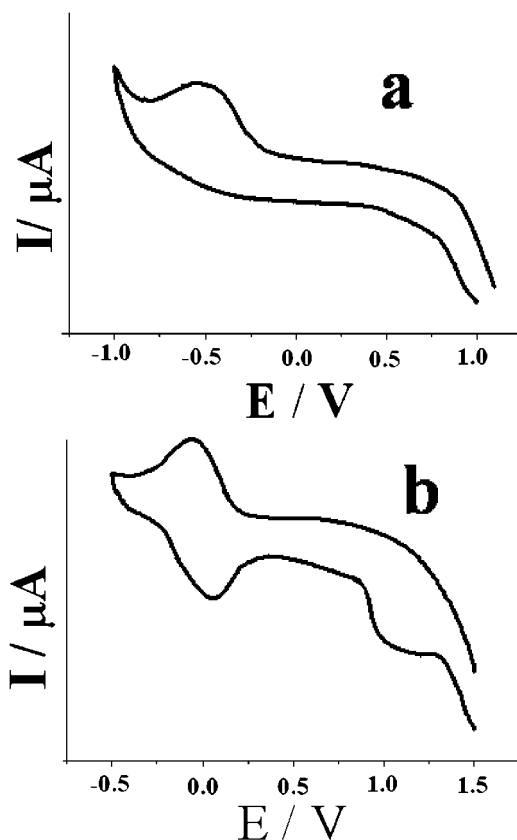
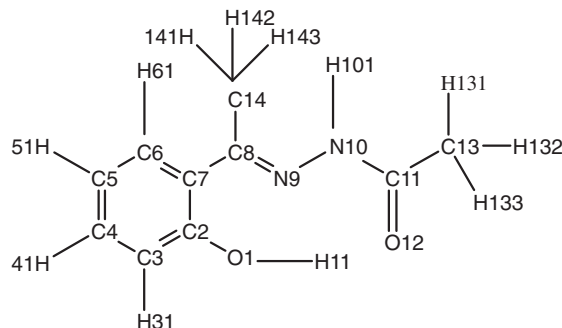


Figure 2. Cyclic voltammogram of **1** (a) and **2** (b).



Scheme 2. Proton numbering scheme for the ${}^1\text{H}$ NMR spectra of LH_2 .

more stabilized and in lower oxidation state than the Mn species.

${}^1\text{H}$ NMR Spectroscopy of the Free Ligand LH_2 . ${}^1\text{H}$ NMR spectroscopy has been used to extract information regarding the exact conformation of the ligand LH_2 in free state. The proton numbering is depicted in Scheme 2 and the NMR spectrum of LH_2 is shown in Figure 3. In the NMR spectrum of the free ligand LH_2 a broad 1H singlet peak was observed due to the amide proton (H101) at 8.64 ppm and another broad 1H singlet was obtained at 11.76 ppm for the phenolic $-\text{OH}$ proton (H11). These two peaks indicate that among the two ionic protons in the ligand one is associated to the phenoxo oxygen and the other to the amido nitrogen atoms, so the other oxygen atom (O12) exists in keto conformation in the free ligand. The broadening of the signals may have occurred due to involve-

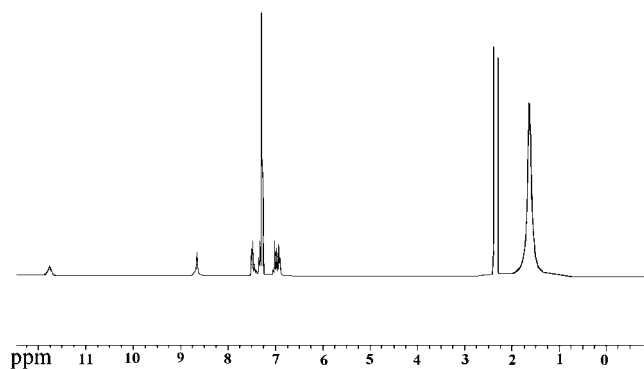


Figure 3. ^1H NMR spectrum of LH_2 .

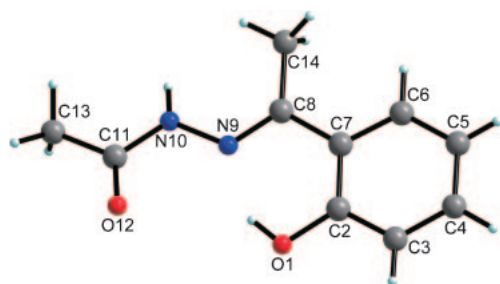


Figure 4. Perspective view of the asymmetric unit of LH_2 .

ment of the protons in intra- and intermolecular hydrogen-bonding interactions.⁵² The methyl protons attached to C13 enjoy deshielding from both O12 and N10 and appear as a 3H singlet at 2.36 ppm and is downfield shifted compared to the methyl protons attached to C14 which undergo paramagnetic deshielding from N9 only and appear as a 3H singlet at 2.32 ppm. Among the aromatic protons H31 being adjacent to the phenolic $-\text{OH}$ group is distinctly deshielded compared to the others and appears as a 1H doublet within 7.46 to 7.49 ppm and the other aromatic protons appear as a multiplet within the region 6.88 to 7.05 ppm. The spectrum of LH_2 contains a broad singlet peak at 1.62 ppm for water molecule and a sharp singlet at 7.26 ppm for CHCl_3 which may be present as impurities. The results obtained from the NMR spectrum are in agreement with the structure of the free ligand obtained by the X-ray analysis (Figure 4).

Crystal Structure of the Free Ligand (LH_2). The single-crystal structure of LH_2 is evaluated in order to establish its actual configuration in metal free state. The asymmetric unit of the free ligand is shown in Figure 4 and the bond lengths and bond angles are listed in Table 3. The asymmetric unit clearly shows that the tridentate Schiff base contains an imine functional group, a phenolic hydroxy group and a secondary amido carbonyl functionality. The phenolic C2–O1 bond distance is 1.356(2) Å, distinctly longer than the ketonic C11–O12 bond distance 1.2200(19) Å. Thus it is evident from the structure that among the two oxygen donor sites of the ONO donor ligand one oxygen is enolic in nature and the other is ketonic.

The crystal packing of LH_2 can be envisaged as a tape-like 1D supramolecular network resulting from intra- and intermolecular hydrogen-bonding interactions shown in Figure 5 and listed in Table 4. The phenolic proton associated with O1 being

Table 3. Selected Bond Distances and Bond Angles of LH_2

Bond lengths/Å		Bond angles/°	
O1–C2	1.356(2)	O1–C2–C3	116.77(15)
C2–C3	1.392(2)	O1–C2–C7	123.06(15)
C2–C7	1.415(2)	C3–C2–C7	120.17(16)
C3–C4	1.371(3)	C2–C3–C4	120.71(16)
C4–C5	1.378(3)	C3–C4–C5	120.21(17)
C5–C6	1.380(3)	C4–C5–C6	119.71(18)
C6–C7	1.396(2)	C5–C6–C7	122.06(16)
C7–C8	1.477(2)	C2–C7–C6	117.13(15)
C8–N9	1.289(2)	C2–C7–C8	121.81(14)
C8–C14	1.496(2)	C6–C7–C8	121.06(14)
N9–N10	1.3701(18)	C7–C8–N9	115.10(13)
N10–C11	1.358(2)	C7–C8–C14	120.55(14)
C11–O12	1.2200(19)	N9–C8–C14	124.34(15)
C11–C13	1.493(2)	C8–N9–N10	121.65(13)
		N9–N10–C11	117.12(12)
		N10–C11–O12	121.22(16)
		N10–C11–C13	115.23(14)
		O12–C11–C13	123.55(16)

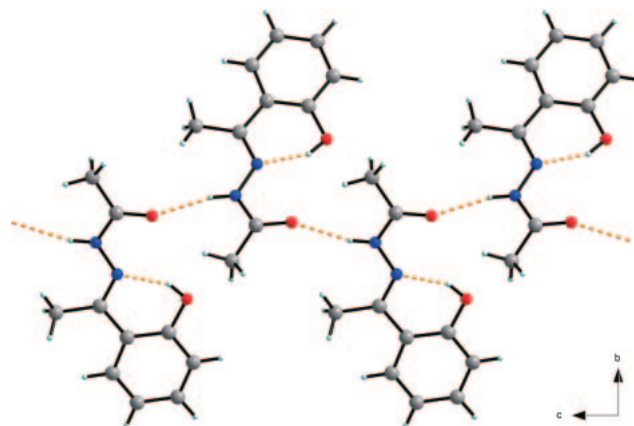


Figure 5. Crystal packing of LH_2 , showing the hydrogen-bonded one-dimensional network.

Table 4. Hydrogen-Bond Parameters for LH_2 , 1, 2, and 3

	D–H...A	d(D–H) /Å	d(H...A) /Å	d(D...A) /Å	∠(DHA) /°
LH_2	N10–H101...O12	0.85	2.07	2.907(3)	166.11
	O1–H11...N9	0.84	1.78	2.532(3)	148.38
Complex 1	N24–H5...O41	0.86	1.97	2.808(7)	166
	O41–H1...O14	0.82	1.90	2.688(7)	162
	C27–H271...O1	0.95	2.44	3.361(7)	163
Complex 2	C6–H6...O26	0.98	2.609	3.486	153
	C27–H27B...O15	0.98	2.53	3.463	158
	C14–H14B...O1	0.98	2.645	3.395	133
Complex 3	N11–H3...O23	0.84	2.13	2.947(7)	164

intramolecularly hydrogen bonded to the imine nitrogen (N9) forms a stable six-membered ring assembly. The secondary amido proton attached to N10 has a favorable orientation to form intermolecular hydrogen bond with the ketonic oxygen (O12) of the adjacent unit and by reiteration of this intermolecular interaction the 1D supramolecular chain-like polymer

resulted along the crystallographic *c* axis. A closer look at the crystal packing reveals that any two adjacent molecules reside in two different planes. Thus every alternative molecule of the polymeric chain defines two molecular planes connected like a hinge at an angle 50.07°.

Crystal Structure of [Co(LH)₂]·CH₃OH (1). The perspective view of **1** is shown in Figure 6 and the bonding parameters are listed in Table 5. In **1** the Co^{II} ion forms the bis-chelated complex with two mono anionic tridentate ONO donor hydrazone ligands. The ligands coordinate the Co^{II} ion via the ketonic oxygen (O1 and O21), the azomethine nitrogens (N5

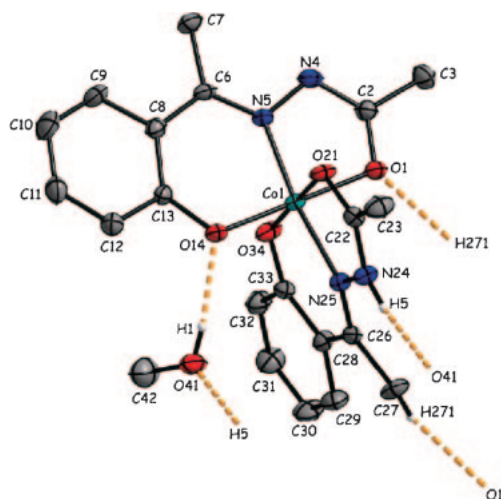


Figure 6. Perspective view of the asymmetric unit of **1**.

and N25) and the deprotonated phenolic oxygens (O14 and O34). The bond dimensions in the two ligands differ slightly in **1** (Table 5) but confirms their coordination via the ketonic form (Form II in Scheme 1). The ligands are disposed around the metal center in meridional orientation with the phenolic and ketonic oxygens *cis* to each other and the azomethine nitrogen atoms *trans*. Thus Co^{II} adopts distorted octahedral coordination geometry. The twelve *cis* angles range from 84.5(1) to 95.7(1)° and the three *trans* angles held by O1–Co1–O14 (179.0(2)°), N5–Co1–N25 (172.2(2)°), and O21–Co1–O34 (178.8(2)°) suggest that these are quite close to the ideal 90 (*cis*) and 180° (*trans*) values of a perfect octahedron. The slight distortion from the idealized geometry may be attributed to the restricted bite angles imposed by the planar tridentate Schiff bases. The phenolic oxygens (O14 and O34) and two ketonic oxygens (O1 and O21) are very close to the mean plane passing through them and define the equatorial plane of the CoN₂O₄ chromophore, while two axial sites are occupied by the two azomethine nitrogen atoms (N5 and N25). The mean planes defined by the donor atoms of the two ligands are almost perfectly orthogonal to each other being inclined at an angle of 89.41°.

The crystal packing of **1** exhibits intermolecular N–H...O, O–H...O, and C–H...O hydrogen bonds shown in Figure 7 and listed in Table 4. The intermolecular hydrogen bonding is mainly assisted by the methanol molecule present in the lattice. Two neighboring monomeric units are linked through methanol molecules by a pair of cooperative hydrogen bonds N24–H5...O41 and O41–H1...O14 with the formation of a

Table 5. Selected Bond Distances and Bond Angles of **1**, **2**, and **3**

1		2		3	
Bond lengths/Å					
Co1–O1	1.875(3)	Mn1–O15	1.8448(17)	Zn1–O1	1.989(2)
Co1–O21	1.923(3)	Mn1–O1	1.8493(17)	Zn1–O14	2.069(2)
Co1–N5	1.861(3)	Mn1–O26	1.9067(17)	Zn1–O1	2.004(2)
Co1–N25	1.902(3)	Mn1–O12	1.9161(18)	Zn1–O21	1.978(2)
Co1–O14	1.868(3)	Mn1–N23	1.959(2)	Zn1–N10	2.101(2)
Co1–O34	1.849(3)	Mn1–N9	1.966(2)	C12–O14	1.241(3)
C2–O1	1.293(5)	C11–O12	1.314(3)		
C22–O21	1.241(5)	C25–O26	1.315(3)		
Bond angles/°					
O1–Co1–N5	84.5(1)	O15–Mn1–O1	88.90(8)	O1–Zn1–O1	78.35(8)
O1–Co1–O14	179.0(2)	O15–Mn1–O26	170.93(8)	O1–Zn1–N10	84.21(9)
N5–Co1–O14	95.7(1)	O1–Mn1–O26	88.42(8)	O1–Zn1–O14	145.0(1)
O1–Co1–O21	90.4(2)	O15–Mn1–O12	89.77(8)	O1–Zn1–O21	104.11(9)
N5–Co1–O21	91.4(1)	O1–Mn1–O12	170.08(7)	N10–Zn1–O21	115.65(9)
O14–Co1–O21	88.6(2)	O26–Mn1–O12	94.33(7)	Zn1–O1–Zn1	100.95(9)
O1–Co1–N25	89.0(1)	O15–Mn1–N23	91.04(8)	O1–Zn1–N10	140.08(9)
N5–Co1–N25	172.2(2)	O1–Mn1–N23	97.43(8)	O1–Zn1–O14	100.20(8)
O14–Co1–N25	90.8(1)	O26–Mn1–N23	80.72(8)	N10–Zn1–O14	78.02(9)
O21–Co1–N25	84.3(1)	O12–Mn1–N23	92.42(8)	O1–Zn1–O21	111.1(1)
O1–Co1–O34	90.3(2)	O15–Mn1–N9	95.09(8)	O14–Zn1–O21	98.5(1)
N5–Co1–O34	89.6(1)	O1–Mn1–N9	90.20(8)		
O14–Co1–O34	90.7(2)	O26–Mn1–N9	93.58(8)		
O21–Co1–O34	178.8(2)	O12–Mn1–N9	80.13(8)		
N25–Co1–O34	94.8(2)	N23–Mn1–N9	170.31(9)		

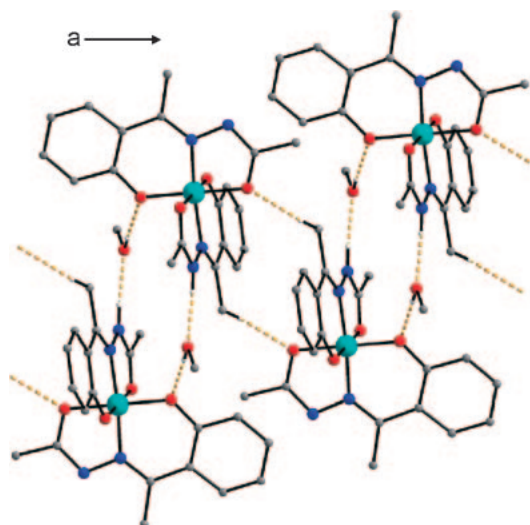


Figure 7. Crystal packing of **1**, showing the methanol mediated centrosymmetric, cooperatively hydrogen-bonded 1D bilayer network.

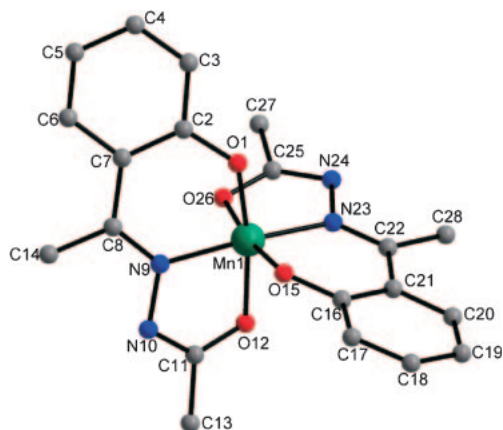


Figure 8. Perspective view of the asymmetric unit of **2**.

centrosymmetric dimer (Symmetry transformation: $-x, -y, -z$). Interaction between two such adjacent dimers is further supported by another centrosymmetric nonclassical C27–H271...O1 hydrogen-bonding interaction along the crystallographic a axis forming a one dimensional bilayer *zig-zag* supramolecular assembly.

Crystal Structure of [Mn(L)₂] (2). **2** consists of a central Mn^{IV} cation surrounded by two dianionic tridentate ONO donor hydrazone ligands (L²⁻) (Figure 8). The bond dimensions of the MnN₂O₄ chromophore are listed in Table 5. The overall geometry about the central Mn ion is octahedral with the meridional disposition of the two tridentate ligands. As in **1**, the mean equatorial plane around the central metal ion in **2** is also formed by the four oxygen atoms and the two azomethine nitrogens occupy the *trans* (axial) positions to complete the octahedron. Unlike in **1**, the ligands in **2** coordinate the Mn ion via the enol tautomeric form and behave as a dianionic species to stabilize the +IV oxidation state of the Mn ion (Form III of Scheme 1). The average Mn–N and Mn–O bond lengths for **2** are 1.9625 and 1.8792 Å, respectively which are in good agreement with those for various reported Mn^{IV} mononuclear

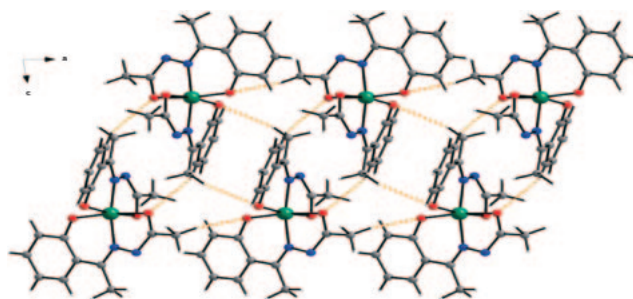


Figure 9. Packing diagram of **2**, showing the zig-zag bilayer 1D supramolecular architecture.

and dinuclear octahedral complexes having MnN₂O₄ core.^{53–55} The O–Mn–O and O–Mn–N *cis* angles have an average value of 90.17° whereas the three *trans* angles deviate by about 10° from ideal 180° value. The angle between the planes defined by the ONO donor sets of the two ligands is 86.75°, close to 90° suggesting that the ligands are essentially orthogonal.

A closer look at the amido C–O bond distance in free LH₂, **1**, and **2** reveals that this distance is 1.315(3) Å in **2**, distinctly longer than the amido C–O linkage in free LH₂ and **1** (1.220(2) and 1.267(5) Å respectively) and confirms the single bond character of this C–O bond in complex **2** in contrast to the double bond features in LH₂ and **1**. Thus quantitative evidence in favor of enolic coordination of amido carbonyl group in **2** and ketonic coordination in **1** can be rationalized. These different coordination modes of the ligand in **1** and **2** are reflected in their hydrogen-bonding patterns. As the ligand in **2** is doubly deprotonated there is no favorable situation for usual N–H...O and O–H...O hydrogen bonding as observed in LH₂ and **1** but the adjacent mononuclear units are close packed through the weak C–H...O interaction shown in Figure S2. Thus three cooperative C–H...O hydrogen-bonding interactions listed in Table 4 generate a bilayer supramolecular chain along the crystallographic a axis in which the mononuclear unit of each layer partly interdigitate between two neighboring units of another layer (Figure 9) to strengthen the supramolecular self-assembly.

Crystal Structure of [Zn(LH)(OOCF₃)₂] (3). The perspective view of the asymmetric unit of the Zn^{II} complex **3** is shown in Figure 10 and the required bond lengths and bond angles are listed in Table 5. **3** encounters a crystallographically imposed rotational symmetry element (C_2 axis) forming a bis(μ_2 -phenoxo) bridged dinuclear structure with each Zn^{II} ion being penta-coordinated sharing two phenoxo oxygens from two symmetry related ligand fragments (Figure S3). It is to be noted here that unlike **1** and **2** the ligand in **3** exhibits the μ_2 -bridging mode of the phenoxo oxygen (Form IV of Scheme 1) which results in an increased nuclearity from mononuclear complexes **1** and **2** to symmetric dinuclear complex **3** along with growing symmetry elements leading to triclinic (**1** and **2**) to monoclinic (**3**) space group. The Zn1 ion in **3** adopts a square-pyramidal geometry as defined by the Addison parameter $\tau = 0.082$, ($\tau = |\beta - \alpha|/60^\circ$ where β and α are the two largest angles around the central atom; $\tau = 0$ and 1 for perfect square-pyramidal and trigonal-bipyramidal geometries, respectively).⁵⁶ The three coordination sites of the equatorial plane defined by O14, N10, O1, and O1 of another

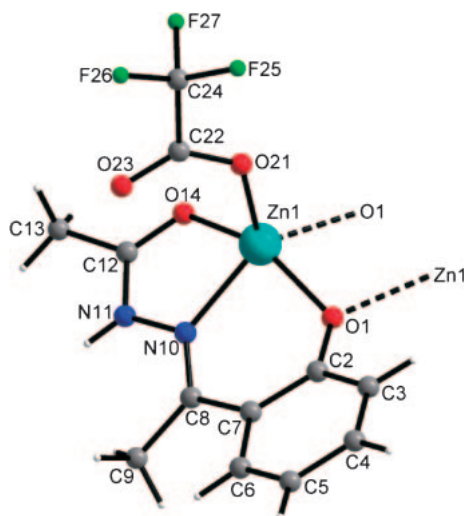


Figure 10. Perspective view of the asymmetric unit of **3**.

unit (symmetry transformation: $-x, y, 1/2 - z$) are occupied by the ONO donor set of the Schiff base ligand. The ONO donor ligand forms a five-membered chelate ring with the help of the keto oxygen (O14) and the imine nitrogen (N10) and a six-membered chelate ring using the imine nitrogen (N10) and bridging phenoxo oxygen (O1) around the metal center Zn1. The fourth equatorial position is blocked by another bridging phenoxo oxygen which actually belongs to the other symmetry related half of the Zn₂ dimer. It is worth mentioning here that the amido carbonyl group involving C12–O14 linkage coordinates the Zn^{II} ion in ketonic form as in **1** and the C–O bond distances in free **LH**₂, **1**, and **3** are quite comparable but differ from those of **2** (Tables 3 and 5). The axial position of the Zn^{II} ion is occupied by the oxygen atom (O21) of a terminally coordinated trifluoroacetate anion. Thus each Zn^{II} ion describes a distorted square-pyramidal geometry within a NO₄ coordination sphere. The distortion from ideal square-pyramidal geometry as evident from the bond dimensions is further supported by the axial displacement of the Zn1 ion from the mean equatorial plane by 0.592 Å. The intradimer Zn...Zn distance is 3.080 Å and is consistent with the reported Zn...Zn separations in double phenoxo-bridged Zn complexes.^{30,57}

A further insight into the intermolecular interaction in **3** exhibits that the discrete butterfly shaped dimeric units are associated through the N–H...O hydrogen bonds (Figure 11 and Table 4) occurring between the amido nitrogen (N11) of one dinuclear unit to the noncoordinated trifluoroacetate oxygen (O23) of the neighboring unit related by glide plane symmetry (*b*_a glide) on either side. Thus the supramolecular self-assembly of **3** can be best described as a 2D (4, 4) grid topology by considering the dinuclear metallo-organic units as a node and the N11–H3...O23 bonds to be linker (Figure 11). The single layer 2D network exhibits supramolecular nanoporosity in the structure having a dimension of 9.524 × 18.369 Å (based on nearest intermolecular Zn...Zn distance along the *b* and *a* axes respectively). A space filling model of the crystal packing (Figure 12) clearly shows the nanopores enclosed by the supramolecular (4, 4) grids.

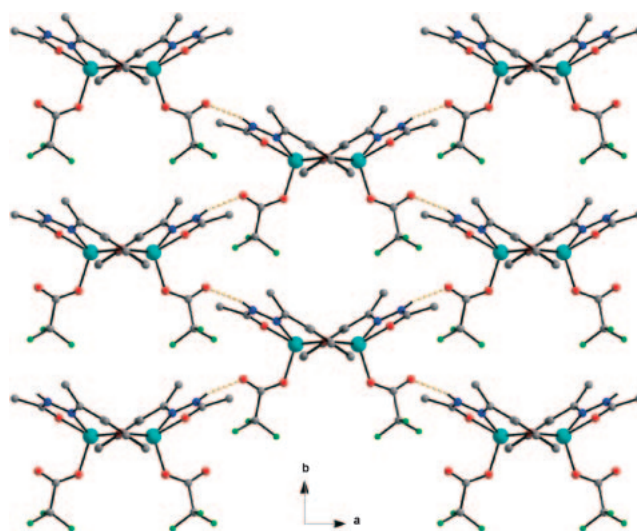


Figure 11. The crystal packing of **3**, showing the (4, 4) grid 2D supramolecular architecture formed by the N–H...O hydrogen-bonding interactions among the butterfly shaped dimeric units related by *b*_a glide plane symmetry.

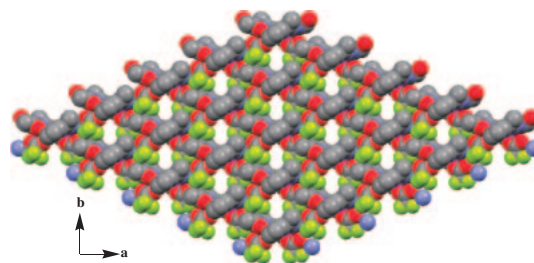


Figure 12. A space filling model of **3**, showing distinctly visible supramolecular nanopores along *c* axis.

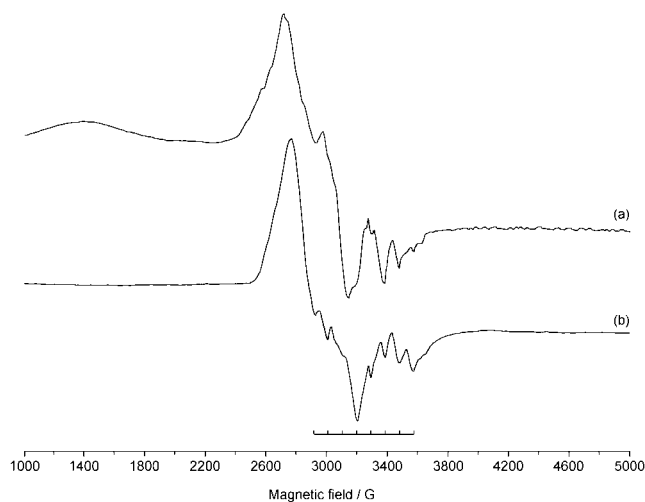


Figure 13. X-band EPR spectra of **1** recorded on the polycrystalline powder (a) at 100 K and (b) at 298 K. With the eight lines is indicated the hyperfine splitting due to ⁵⁹Co nucleus.

EPR Spectroscopic Studies of 1 and 2. EPR spectra of **1** recorded on polycrystalline powder are characterized by a similar pattern from 100 to 298 K (Figure 13). They appear to be close to axial symmetry with a negligible rhombicity. The *g*

values measured at liquid nitrogen temperature are $g_{\perp} = 2.363$ and $g_{\parallel} = 2.016$. The spectral features support a low-spin d^7 configuration with the unpaired electron in the d_{z^2} orbital. On the whole, the spectra closely resemble those for other low-spin Co^{II} species with axial or slight rhombic symmetry.^{58–65} Theoretical treatments of the spin Hamiltonian parameters for such situations have been developed by several authors, in which g (and A) values can be related to the ground-state electronic configuration and the energy separation of the low-lying doublet (2A_1) and the quartet excited states;^{66–68} up to first order approximation g values can be expressed by the following equations:

$$g_{\perp} = g_e + \frac{6\lambda}{\Delta E} > 2.0023 \quad (3)$$

$$g_{\parallel} = g_e \approx 2.0023 \quad (4)$$

where λ is the spin-orbit coupling (higher than 0 for a d^7 configuration) and ΔE is the energy difference between the set (d_{yz}, d_{xz}) and d_{z^2} orbital.⁶⁹ From eqs 3 and 4, it emerges that $g_{\perp} > g_{\parallel} \approx 2$, in agreement with the experimental observations.

At liquid nitrogen temperature, the coupling between the unpaired electron and ${}^{59}\text{Co}$ nucleus (characterized by nuclear spin number $I = 7/2$ and natural abundance of 100%) is detected; owing to such an interaction, it is expected that each transition splits into $2I + 1 = 8$ lines. They can be resolved around the parallel region and appears partly observable in the perpendicular region; the approximated A_{\parallel} of $96 \times 10^{-4} \text{ cm}^{-1}$ is compatible with the structure of **1** and with the data reported in the literature.^{58,59,62,64} No hyperfine coupling with ${}^{14}\text{N}$ nuclei is observed. EPR spectrum at room temperature (Figure 13b) also displays a very broad signal centered at 1380 Gauss with $g \approx 4.74$; this is possibly due to a high-spin Co^{II} contribution that occurs with increasing temperature: the value of $g > 4$ is characteristic of such electronic configurations.^{70–75}

EPR spectra of **1** dissolved in coordinating (DMF), slightly coordinating (CH_3CN) or in noncoordinating solvents (mixture $\text{CH}_2\text{Cl}_2/\text{toluene}$ 50/50 v:v) are comparable with those recorded on the powder and demonstrate that the solid-state structure is retained in solution.

The X-band EPR spectrum recorded on a polycrystalline sample of **2** is displayed in Figure 14a. The major feature of the spectrum is a strong and well-defined $g \approx 2$ resonance and a weak, broad signal at low field. The complexity of interpreting the EPR spectra of d^3 (Mn^{IV} and Cr^{III}) ions depending on the magnitude of the zero-field splitting D and rhombic distortion E has been widely discussed in the literature.^{76–78} Such a complexity can be simplified in an axial field ($E/D = 0$) and when the axial D is either much larger ($2D \gg h\nu$) or much smaller ($2D \ll h\nu$) than the applied microwave frequency. In the first case two signals occur, with the first being a strong transition at the low field and the second a weaker $g \approx 2$ component. This observation is true for Mn^{IV} complexes like MnO_6 formed by catecholate⁷⁹ and sorbitolate,⁸⁰ MnN_4O_2 formed by hexadentate amide-amino-phenolate,⁸¹ and MnN_2O_4 formed by hydroxyphenyl-imino-phenolate ligand.⁸² In the second case, when D is small, the $g \approx 2$ signal dominates with relatively weak low-field signals. This is observed for thiohydroxamate⁸³ and dithiocarbamate⁸⁴ Mn^{IV} species. The EPR spectra become isotropic when the extreme limit of $D = 0$

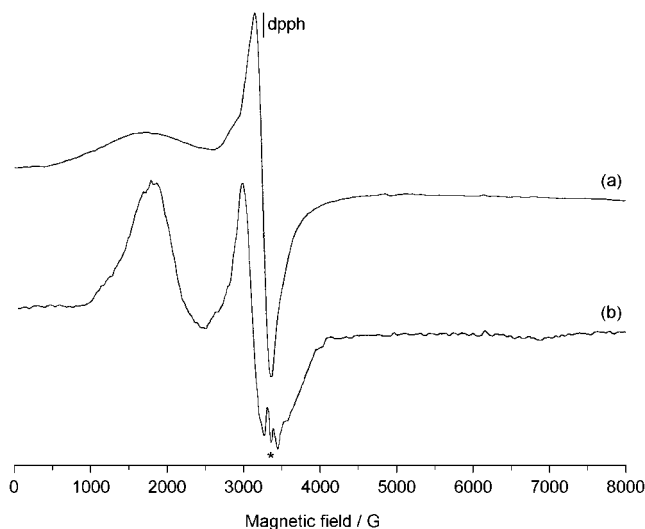


Figure 14. X-band EPR spectra of **2** at room temperature, (a) recorded on the polycrystalline powder and (b) in CH_3CN . With the asterisk is indicated the hyperfine splitting due to ${}^{55}\text{Mn}$ nucleus.

is reached, exhibiting a strong signal at $g \approx 2$ region. **2** shows a strong band at $g = 2.01$ and a weak band at $g = 3.78$; therefore, it belongs to the second situation described above and $D \ll 0.15 \text{ cm}^{-1}$ ($h\nu \approx 0.31 \text{ cm}^{-1}$ at X-band frequencies). A simulation of the spectrum suggests that D is around 0.08 cm^{-1} and E/D around 0.14; the value of $E \neq 0$ can be explained with the rhombicity of the molecular geometry of **2** ($\text{Mn-O1(O15)} \approx 1.85$, $\text{Mn-O12(O26)} \approx 1.91$, and $\text{Mn-N9(N23)} \approx 1.96 \text{ \AA}$).

The features are retained in the organic solvents, and the spectrum recorded in CH_3CN is shown in Figure 14b. Analogous signals are obtained in DMF or in a mixture $\text{CH}_2\text{Cl}_2/\text{toluene}$ 50/50 v:v. In the solution too, all the lines are extremely broad; as a consequence, no ${}^{55}\text{Mn}$ hyperfine splitting was observable in the band at lower field and only three of the six expected transitions can be observed in the broad resonance centered at $g \approx 2$ (indicated by an asterisk in Figure 14b): however the magnitude of the ${}^{55}\text{Mn}$ hyperfine coupling (79 G) is consistent with previous reports for the Mn^{IV} species.⁸⁵ For example, for the compound $[\text{Mn}(\text{salahp})]$, where H_2salahp is 1-hydroxy-3-salicylideneaminopropane, with identical MnO_4N_2 coordination and [(O(phen), N(imine), and O(alk))] donor set, a value of 77 G has been reported.^{24,86,87} Thus, both the spectra recorded on the solid sample and in solution support an oxidation state of +IV for manganese.

Fluorescence Spectroscopic Study of LH_2 and **3.** The steady state fluorescence emission spectra of the free ligand LH_2 and the zinc complex **3** in acetonitrile solution at room temperature are shown in Figure 15. For the free ligand LH_2 ($\lambda_{\text{ex}} = 320 \text{ nm}$) there is a broad emission band at 449 nm. Upon excitation in the UV region, **3** ($\lambda_{\text{ex}} = 356 \text{ nm}$) exhibits a narrow emission band with the maximum at 468 nm and a tail extending up to 600 nm, indicating that it is a typical blue emitter. A similar emission pattern, characteristic of imino-phenolate complexes was also recently observed.^{24,29,30,86,87} The emission maximum of **3** is distinctly (19 nm) red shifted

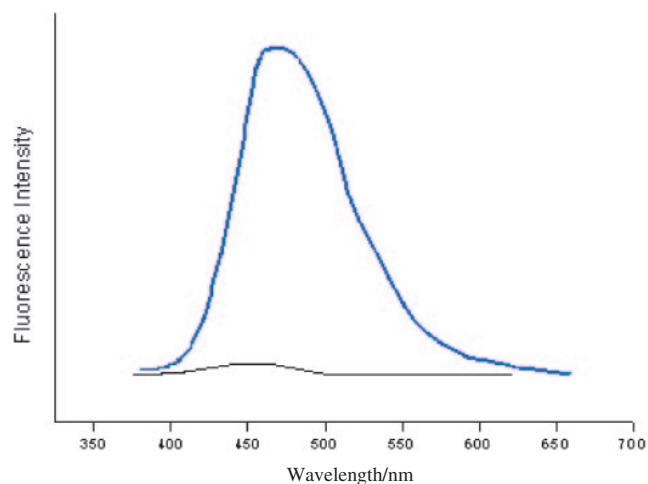


Figure 15. Emission spectra of **LH₂** (black line) and **3** (blue line) in CH₃CN following excitation at 320 and 356 nm for **LH₂** and complex **3** respectively.

compared to the free ligand. The calculated fluorescence quantum yield of **3** is 40.43%, significantly higher than that recorded for the free ligand (0.15%).

Luminescence properties of Zn^{II} complexes originate from the organic ligand rather than LMCT because the d shell of the central ion is completely filled.⁸⁸ Therefore the large increase in emission intensity and ≈ 270 times enhancement of fluorescence quantum yield of **3** compared to the free ligand **LH₂** can be rationalized by the presence of the zinc atom. The metal plays a pivotal role in increasing the conformational rigidity and the extent of conjugation of the ligand, thus restricting energy loss via nonradiative decay such as vibrational motions and/or photoinduced electron transfer (PET)⁸⁹ leading to a bright and intense emission. The hydrogen-bonding interaction in the free ligand leads to 1D chain-like assembly whereas it clips the complex molecules in **3** into a 2D supramolecular sheet in the ground state. The hydrogen-bonding interactions are expected to be stronger with increasing dipole moment of the molecules in the excited state and stabilize the excited state of the species.⁹⁰ But in solution state there is another competitive influence of solvent molecules. The solvent molecules may participate in hydrogen bonding with the luminescent species and quench its luminescent properties by bond vibration and other nonradiative processes. For complexes [Co(**LH₂**)₂]·CH₃OH (**1**) and [Mn(**L₂**)] (**2**) no fluorescence emission spectra can be observed though the metal ions play the same pivotal role as the Zn^{II} ion in **3** and impose conformational rigidity to the ligand. Here the transition metal (Co/Mn)–fluorophore (F) electron/energy transfer interaction and d–d electronic transition results in quenching of fluorescence.^{91,92}

Time-resolved luminescence measurement of **3** allowed the intensity of the emission after a laser excitation pulse at 370 nm to be followed. The decay shown in Figure S4 is clearly double exponential. The decay function can be described by a fast lifetime component $\tau_{\text{fast}} = 0.98$ ns and a slow lifetime component $\tau_{\text{slow}} = 2.93$ ns.

The steady state fluorescence emission spectra of the free ligand **LH₂** and the zinc complex **3** have been measured in the

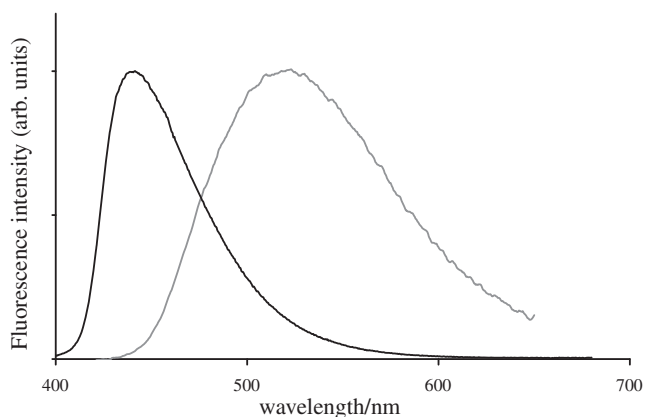


Figure 16. Solid-state fluorescence spectra of **3** (dark, $\lambda_{\text{exc}} = 356$ nm) and **LH₂** (gray, $\lambda_{\text{exc}} = 320$ nm).

solid state at room temperature using a multichannel spectrometer fitted with an integrating sphere and are depicted in Figure 16.

Upon excitation at 356 nm, **3** exhibits a narrow emission band centered at 440 nm and a tail extending up to 600 nm. This emission pattern is very similar to the one previously recorded in acetonitrile solution but with a hypsochromic shift of the maximum of emission of 28 nm possibly due to stacking interactions in the solid state. A similar emission pattern had also been recently recorded for a dicyanoamide-bridged 2D polynear Zn^{II} complex.⁹³

Upon excitation at 320 nm, **LH₂** exhibits a broad emission spectrum with a maximum at 521 nm (Figure 16). This spectrum differs significantly from the emission pattern observed in acetonitrile solution, as a strong bathochromic shift of 72 nm is observed. This is indicative of strong intermolecular interactions in the solid state, as for instance, the noncovalent interactions, the formation of excimers or exciplexes.

The fluorescence quantum yields of **LH₂** and **3** have been measured in the solid state with an absolute method based on the use of the integrating sphere. The calculated fluorescence quantum yield of **3** is 18%, which is twice lower than the value obtained in acetonitrile and which may be attributed to self-absorption processes.

In contrast, the ligand **LH₂** displays a much higher quantum yield in the solid state (25%) than in acetonitrile solution (0.15%). It is surmised that the restricted motions in the solid state drastically reduce the vibrational quenching phenomena such as excited state proton transfer often observed with salicylaldehyde⁹⁴ and salicylideneaniline.⁹⁵

Conclusion

In conclusion this paper describes the differing coordination behavior of an ONO donor hydrazone Schiff base ligand in the presence of different metal ions. In its free state the ligand is monobasic and shows interesting 1D supramolecular chain-like assembly. In **1** the ligand coordinates in its tridentate mono-negative keto form to stabilize the +II oxidation state of a cobalt ion. In **2** the amido carbonyl group of the ligand undergoes enolisation along with further deprotonation and thus the ligand stabilizes the +IV oxidation state of a

manganese ion. Apart from different oxidation states the ligand also exhibits a variety of chelating properties. In **1** and **2** it coordinates the metal ions via tridentate terminal fashion leading to distorted octahedral bis chelate complexes, but in **3** the ligand shows tridentate bridging mode which leads to a bis(μ_2 -phenoxo)-bridged dinuclear square-pyramidal Zn^{II} complex containing crystallographically imposed rotational symmetry (C_2). All three complexes form supramolecular networks via N–H...O, O–H...O, and C–H...O hydrogen bonds among which the single layer 2D supramolecular (4, 4) grid network of **3** shows nanoporous characteristics.

Emphasis has been given in this work upon the different spectroscopic characterization and applications of the complexes along with the ligand. Apart from the routine IR, UV–vis spectroscopy **LH₂** was characterized by ¹H NMR spectroscopy which supports the ketonic form of the amido carbonyl functionality of the ligand in free state. The complexes **1** and **2** were characterized by cyclic voltammetry and EPR spectroscopy. The X-band EPR spectra confirm the presence of the cobalt ion in low-spin +II oxidation state and manganese ion in +IV oxidation state, thus supporting the monoanionic and dianionic coordination behavior of the ligand in the respective complexes. The luminescence spectrum of **3** with respect to the free ligand shows that **3** is a typical blue emitter. The ligand shows much enhanced luminescence in solid state compared to solution state due to predominant intermolecular interaction but this phenomenon is reversed in the case of **3** probably due to self absorption process in solid state.

D. Sadhukhan is thankful to University Grants Commission, New Delhi, Government of India and S. Mitra acknowledges Council of Scientific and Industrial Research, New Delhi, Govt. of India for providing financial support to carry out this work. The authors are also thankful to Mr. S. Roy, Dr. C. R. Sinha, and Dr. N. Chattopadhyay, Department of Chemistry, Jadavpur University, Kolkata, India for helping in the fluorescence study.

Supporting Information

It contains the FT-IR spectrum of **1** (Figure S1), the figure presenting the H-bonds in **2** (Figure S2), the symmetric dimeric view of **3** (Figure S3), and the time-resolved emission decay curve of **3** (Figure S4). This materials are available free of charge on the web at <http://www.csj.jp/journals/bcsj/>.

References

- 1 L. Antolini, L. P. Battaglia, A. B. Corradi, G. Marcotrigiano, L. Menabue, G. C. Pellacani, *J. Am. Chem. Soc.* **1985**, *107*, 1369.
- 2 S. Naskar, D. Mishra, S. K. Chattopadhyay, M. Corbella, A. J. Blake, *Dalton Trans.* **2005**, 2428.
- 3 A. Ray, C. Rizzoli, G. Pilet, C. Desplanches, E. Garribba, E. Rentschler, S. Mitra, *Eur. J. Inorg. Chem.* **2009**, 2915.
- 4 S. Patai, *The Chemistry of the Carbon-Nitrogen Double Bond*, Interscience, New York, **1970**.
- 5 J. R. Merchant, D. S. Chothia, *J. Med. Chem.* **1970**, *13*, 335.
- 6 J. R. Dilworth, *Coord. Chem. Rev.* **1976**, *21*, 29.
- 7 S. Banerjee, S. Mondal, S. Sen, S. Das, D. L. Hughes, C. Rizzoli, C. Desplanches, C. Mandal, S. Mitra, *Dalton Trans.* **2009**, 6849.
- 8 S. Banerjee, S. Mondal, W. Chakraborty, S. Sen, R. Gachhui, R. J. Butcher, A. M. Z. Slawin, C. Mandal, S. Mitra, *Polyhedron* **2009**, *28*, 2785.
- 9 S. Sridhar, M. Saravanan, A. Ramesh, *Eur. J. Med. Chem.* **2001**, *36*, 615.
- 10 B. Bottari, R. Maccari, F. Monforte, R. Ottanà, E. Rotondo, M. Vigorita, *Bioorg. Med. Chem. Lett.* **2000**, *10*, 657.
- 11 B. K. Kaymakçioğlu, S. Rollas, *Farmaco* **2002**, *57*, 595.
- 12 E. W. Ainscough, A. M. Brodie, J. D. Ranford, J. M. Waters, *Inorg. Chim. Acta* **1995**, *236*, 83.
- 13 E. W. Ainscough, A. M. Brodie, A. J. Dobbs, J. D. Ranford, J. M. Waters, *Inorg. Chim. Acta* **1998**, *267*, 27.
- 14 J. Easmon, G. Puerstinger, T. Roth, H. Fiebig, M. Jenny, W. Jaeger, G. Heinisch, J. Hofmann, *Int. J. Cancer* **2001**, *94*, 89.
- 15 L. Sacconi, *J. Am. Chem. Soc.* **1952**, *74*, 4503.
- 16 J. Chakraborty, S. Thakurta, G. Pilet, D. Luneau, S. Mitra, *Polyhedron* **2009**, *28*, 819.
- 17 B. Mondal, M. G. B. Drew, T. Ghosh, *Inorg. Chim. Acta* **2009**, *362*, 3303.
- 18 B. Mondal, T. Ghosh, M. Sutradhar, G. Mukherjee, M. G. B. Drew, T. Ghosh, *Polyhedron* **2008**, *27*, 2193.
- 19 P. B. Sreeja, M. R. P. Kurup, A. Kishore, C. Jasmin, *Polyhedron* **2004**, *23*, 575.
- 20 A. Ray, S. Banerjee, R. J. Butcher, C. Desplanches, S. Mitra, *Polyhedron* **2008**, *27*, 2409.
- 21 S. Sen, C. R. Choudhury, P. Talukder, S. Mitra, M. Westerhausen, A. N. Kneifel, C. Desplanches, N. Daro, J.-P. Sutter, *Polyhedron* **2006**, *25*, 1271.
- 22 S. Pal, S. Pal, *Eur. J. Inorg. Chem.* **2003**, 4244.
- 23 C. W. Tang, S. A. VanSlyke, *Appl. Phys. Lett.* **1987**, *51*, 913.
- 24 T. Yu, W. Su, W. Li, Z. Hong, R. Hua, M. Li, B. Chu, B. Li, Z. Zhang, Z. Z. Hu, *Inorg. Chim. Acta* **2006**, *359*, 2246.
- 25 V. Liuzzo, W. Oberhauser, A. Pucci, *Inorg. Chem. Commun.* **2010**, *13*, 686.
- 26 V. V. Lukov, V. A. Kogan, S. I. Levchenkov, L. V. Zavada, K. A. Lyssenko, O. V. Shishkin, *Zh. Neorg. Khim.* **1998**, *43*, 421.
- 27 F. B. Tamboura, M. Gaye, A. S. Sall, A. H. Barry, Y. Bah, *Acta Crystallogr., Sect. E* **2009**, *65*, m160.
- 28 S. C. Chan, L. L. Koh, P.-H. Leung, J. D. Ranford, K. Y. Sim, *Inorg. Chim. Acta* **1995**, *236*, 101.
- 29 C. Maxim, T. D. Pasatoiu, V. C. Kravtsov, S. Shova, C. A. Muryn, R. E. P. Winpenny, F. Tuna, M. Andruh, *Inorg. Chim. Acta* **2008**, *361*, 3903.
- 30 P. Roy, K. Dhara, M. Manassero, P. Banerjee, *Inorg. Chim. Acta* **2009**, *362*, 2927.
- 31 C. A. Heller, R. A. Henry, B. A. McLaughlin, D. E. Bliss, *J. Chem. Eng. Data* **1974**, *19*, 214.
- 32 H. Ishida, S. Tobita, Y. Hasegawa, R. Katoh, K. Nozaki, *Coord. Chem. Rev.* **2010**, *254*, 2449.
- 33 L. S. Rohwer, J. E. Martin, *J. Lumin.* **2005**, *115*, 77.
- 34 *Xcalibur*, Oxford-Diffraction, **2002**.
- 35 Z. Otwinowski, W. Minor, in *Methods in Enzymology: Macromolecular Crystallography, Part A*, ed. by C. W. Carter, Jr., R. M. Sweet, Academic Press, New York, **1997**, Vol. 276, pp. 307–326.
- 36 A. Altomare, M. C. Burla, M. Camalli, G. L. Cascarano, C. Giacovazzo, A. Guagliardi, A. G. G. Moliterni, G. Polidori, R. Spagna, *J. Appl. Crystallogr.* **1999**, *32*, 115.

- 37 D. J. Watkin, C. K. Prout, J. R. Carruthers, P. W. Betteridge, *CRISTAL, Issue 11*, Chemical Crystallography Laboratory, Oxford, UK, **1999**.
- 38 *CrysAlis-RED 170*, Oxford-Diffraction, **2002**.
- 39 *Area-Detector Integration Software*, Siemens Industrial Automation, Inc., Madison, WI, **1995**.
- 40 *APEX2 Version 2.1: Area Detector Control and Integration Software*, v. 6.45, Bruker Analytical X-ray Instruments, Inc., Madison, WI, USA, **2006**.
- 41 G. M. Sheldrick, *Acta Crystallogr., Sect. A* **2008**, *64*, 112.
- 42 L. J. Farrugia, *J. Appl. Crystallogr.* **1999**, *32*, 837.
- 43 C. T. Yang, B. Moubaraki, K. S. Murray, J. D. Ranford, J. J. Vittal, *Inorg. Chem.* **2001**, *40*, 5934.
- 44 K. Nakamoto, *Infrared and Raman Spectra of Inorganic and Coordination Compounds: Part A: Theory and Applications in Inorganic Chemistry*, 5th ed., John Wiley & Sons, Inc., New York, **1997**, p. 23.
- 45 Z. H. Sun, D. Xu, X. Q. Wang, G. H. Zhang, G. Yu, L. Y. Zhu, H. L. Fan, *Mater. Res. Bull.* **2009**, *44*, 925.
- 46 A. Ray, G. M. Rosair, R. Kadam, S. Mitra, *Polyhedron* **2009**, *28*, 796.
- 47 D. N. Kumar, B. S. Garg, *J. Therm. Anal. Calorim.* **2002**, *69*, 607.
- 48 K. Nakamoto, M. Suzuki, T. Ishiguro, M. Kozuka, Y. Nishida, S. Kida, *Inorg. Chem.* **1980**, *19*, 2822.
- 49 D. M. Sherman, *Am. Mineral.* **1984**, *69*, 788.
- 50 A. B. P. Lever, *Inorganic Electronic Spectroscopy*, Elsevier, Amsterdam, **1984**, p. 553.
- 51 R. A. Lal, S. Bhaumik, A. Lemtur, M. K. Singh, D. Basumatari, S. Choudhury, A. De, A. Kumar, *Inorg. Chim. Acta* **2006**, *359*, 3105.
- 52 W. Kemp, *Organic Spectroscopy*, 3rd ed., Palgrave Publishers, **1991**.
- 53 H. Torayama, T. Nishide, H. Asada, M. Fujiwara, T. Matsushita, *Polyhedron* **1998**, *17*, 105.
- 54 H. Torayama, H. Asada, M. Fujiwara, T. Matsushita, *Polyhedron* **1999**, *17*, 3859.
- 55 C. P. Pradeep, T. Htwe, P. S. Zacharias, S. K. Das, *New J. Chem.* **2004**, *28*, 735.
- 56 A. W. Addison, T. N. Rao, J. Reedijk, J. V. Rijn, G. C. Verschoor, *J. Chem. Soc., Dalton Trans.* **1984**, 1349.
- 57 J. S. Matalobos, A. M. García-Deibe, M. Fondo, D. Navarro, M. R. Bermejo, *Inorg. Chem. Commun.* **2004**, *7*, 311.
- 58 C. Busetto, F. Cariati, P. Fantucci, D. Galizzioli, F. Morazzoni, *J. Chem. Soc., Dalton Trans.* **1973**, 1712.
- 59 F. Cariati, D. Galizzioli, F. Morazzoni, C. Busetto, *J. Chem. Soc., Dalton Trans.* **1975**, 556.
- 60 A. Pezeshk, F. T. Greenway, G. Vincow, *Inorg. Chem.* **1978**, *17*, 3421.
- 61 D. Reinen, A. Ozarowski, B. Jakob, J. Pebler, H. Stratemeier, K. Wiegardt, I. Tolksdorf, *Inorg. Chem.* **1987**, *26*, 4010.
- 62 K. Drabent, J. A. Wolny, M. F. Rudolf, P. J. Chmielewski, *Polyhedron* **1992**, *11*, 271.
- 63 J. Faus, M. Julve, F. Lloret, M. C. Muñoz, *Inorg. Chem.* **1993**, *32*, 2013.
- 64 B. Ramdhanie, J. Telser, A. Caneschi, L. N. Zakharov, A. L. Rheingold, D. P. Goldberg, *J. Am. Chem. Soc.* **2004**, *126*, 2515.
- 65 A. Huber, L. Müller, H. Elias, R. Klement, M. Valko, *Eur. J. Inorg. Chem.* **2005**, 1459.
- 66 B. R. McGarvey, *Can. J. Chem.* **1975**, *53*, 2498.
- 67 W. C. Lin, *Inorg. Chem.* **1976**, *15*, 1114.
- 68 W. C. Lin, P. W. Lau, *J. Am. Chem. Soc.* **1976**, *98*, 1447.
- 69 R. S. Drago, *Physical Methods in Chemistry*, Saunders, Philadelphia, **1977**.
- 70 R. H. Niswander, L. T. Taylor, *J. Am. Chem. Soc.* **1977**, *99*, 5935.
- 71 L. Banci, A. Bencini, C. Benelli, D. Gatteschi, C. Zanchini, *Struct. Bonding (Berlin, Ger.)* **1982**, *52*, 37.
- 72 K. J. Berry, F. Moya, K. S. Murray, A. V. Bergen, B. O. West, *J. Chem. Soc., Dalton Trans.* **1982**, 109.
- 73 J. Zarembowitch, O. Kahn, *Inorg. Chem.* **1984**, *23*, 589.
- 74 P. Thuéry, J. Zarembowitch, *Inorg. Chem.* **1986**, *25*, 2001.
- 75 A. C. Rizzi, C. D. Brondino, R. Calvo, R. Baggio, M. T. Garland, R. E. Rapp, *Inorg. Chem.* **2003**, *42*, 4409.
- 76 S. Pal, P. Ghosh, A. Chakravorty, *Inorg. Chem.* **1985**, *24*, 3704.
- 77 E. Pedersen, H. Toftlund, *Inorg. Chem.* **1974**, *13*, 1603.
- 78 J. C. Hempel, L. O. Morgan, W. B. Lewis, *Inorg. Chem.* **1970**, *9*, 2064.
- 79 K. D. Magers, C. G. Smith, D. T. Sawyer, *Inorg. Chem.* **1980**, *19*, 492.
- 80 D. T. Richens, D. T. Sawyer, *J. Am. Chem. Soc.* **1979**, *101*, 3681.
- 81 S. K. Chandra, A. Chakravorty, *Inorg. Chem.* **1992**, *31*, 760.
- 82 T. M. Rajendiran, J. W. Kampf, V. L. Pecoraro, *Inorg. Chim. Acta* **2002**, *339*, 497.
- 83 K. L. Brown, R. M. Golding, P. C. Healy, K. J. Jessop, W. C. Tennant, *Aust. J. Chem.* **1974**, *27*, 2075.
- 84 P. G. Rasmussen, K. M. Beem, E. J. Hornyak, *J. Chem. Phys.* **1969**, *50*, 3647.
- 85 D. P. Kessissoglou, X. Li, W. M. Butler, V. L. Pecoraro, *Inorg. Chem.* **1987**, *26*, 2487.
- 86 O. Kotova, S. Semenov, S. Eliseeva, S. Troyanov, K. Lyssenko, N. Kuzmina, *Eur. J. Inorg. Chem.* **2009**, 3467.
- 87 S. Basak, S. Sen, S. Banerjee, S. Mitra, G. Rosair, M. T. G. Rodriguez, *Polyhedron* **2007**, *26*, 5104.
- 88 J. He, Y.-G. Yin, X.-C. Huang, D. Li, *Inorg. Chem. Commun.* **2006**, *9*, 205.
- 89 A. Majumder, G. M. Rosair, A. Mallick, N. Chattopadhyay, S. Mitra, *Polyhedron* **2006**, *25*, 1753.
- 90 S. Das, P. K. Bharadwaj, *Cryst. Growth Des.* **2006**, *6*, 187.
- 91 P. S. Zhao, H. Y. Wang, J. Song, L. D. Lu, *Struct. Chem.* **2010**, *21*, 977.
- 92 K. Dhara, S. Karan, J. Ratha, P. Roy, G. Chandra, M. Manassero, B. Mallik, P. Banerjee, *Chem.—Asian J.* **2007**, *2*, 1091.
- 93 D. Sadhukhan, A. Ray, G. Rosair, L. Charbonnière, S. Mitra, *Bull. Chem. Soc. Jpn.* **2011**, *84*, 211.
- 94 L. Rodríguez-Santiago, M. Sodupe, A. Oliva, J. Bertran, *J. Am. Chem. Soc.* **1999**, *121*, 8882.
- 95 S. Mitra, N. Tamai, *Chem. Phys. Lett.* **1998**, *282*, 391.